AFRL-ML-WP-TP-2006-506

EFFECT OF STRAIN-PATH REVERSAL ON MICROSTRUCTURE EVOLUTION AND CAVITATION DURING HOT TORSION TESTING OF Ti-6A1-4V (Preprint)

S.L. Semiatin and P.D. Nicolaou

OCTOBER 2006

Approved for public release; distribution is unlimited.

STINFO COPY

MATERIALS AND MANUFACTURING DIRECTORATE
AIR FORCE RESEARCH LABORATORY
AIR FORCE MATERIEL COMMAND
WRIGHT-PATTERSON AIR FORCE BASE, OH 45433-7750

REPORT DOCUMENTATION PAGE

Form Approved
OMB No. 0704-0188

1. REPORT DATE *(DD-MM-YY)*	2. REPORT TYPE	3. DATES COVERED *(From - To)*
October 2006	Journal Article Preprint	

4. TITLE AND SUBTITLE
EFFECT OF STRAIN-PATH REVERSAL ON MICROSTRUCTURE EVOLUTION AND CAVITATION DURING HOT TORSION TESTING OF Ti-6A1-4V (Preprint)

5a. CONTRACT NUMBER
In House

5b. GRANT NUMBER

5c. PROGRAM ELEMENT NUMBER
62102F

6. AUTHOR(S)
S.L. Semiatin (Metals Branch, Processing Section (AFRL/MLLMP))
P.D. Nicolaou (UES, Inc.)

5d. PROJECT NUMBER
4347

5e. TASK NUMBER
RG

5f. WORK UNIT NUMBER
M02R2000

7. PERFORMING ORGANIZATION NAME(S) AND ADDRESS(ES)

Metals Branch, Processing Section (AFRL/MLLMP)
Metals, Ceramics and Nondestructive Evaluation Division
Materials and Manufacturing Directorate
Air Force Research Laboratory, Air Force Materiel Command
Wright-Patterson AFB, OH 45433-7750

UES, Inc.

8. PERFORMING ORGANIZATION REPORT NUMBER
AFRL-ML-WP-TP-2006-506

9. SPONSORING/MONITORING AGENCY NAME(S) AND ADDRESS(ES)
Materials and Manufacturing Directorate
Air Force Research Laboratory
Air Force Materiel Command
Wright-Patterson AFB, OH 45433-7750

10. SPONSORING/MONITORING AGENCY ACRONYM(S)
AFRL-ML-WP

11. SPONSORING/MONITORING AGENCY REPORT NUMBER(S)
AFRL-ML-WP-TP-2006-506

12. DISTRIBUTION/AVAILABILITY STATEMENT
Approved for public release; distribution is unlimited.

13. SUPPLEMENTARY NOTES
Submitted for publication in the Metallurgical and Materials Transactions, publisher - The Minerals, Metals & Materials Society (TMS). © 2006 TMS. PAO Case Number: AFRL/WS 06-2604, 02 November 2006.

14. ABSTRACT
Hot torsion testing comprising multiple twist reversals was used to establish the effect of strain-path changes on concurrent dynamic globularization and cavitation of Ti-6Al-4V with a colony-alpha starting microstructure. Optical microscopy was used to quantify the cavity area fraction and the effect of globularization on cavitation. The deformation of the hard and soft colonies surrounding the largest cavities and self-consistent-model calculations of strain partitioning were used to estimate the macroscopic and local strains at which colonies with different strengths globularize. It was found that both hard and soft colonies undergo dynamic globularization at the same local strain (i.e., strain within the colony). In addition, cavitation behavior during torsion with multiple strain-path changes was interpreted by taking into account the break up of the colonies into a globular structure. It was found that cavity growth (or shrinkage) persisted as long as there was a flow-stress difference in adjacent regions/colonies surrounding a given cavity. When the microstructure became uniform (as in the case of full globularization), the cavity area fraction did not change measurably with subsequent additional deformation.

15. SUBJECT TERMS
Cavitation, dynamic globularization, hot torsion testing

16. SECURITY CLASSIFICATION OF:			17. LIMITATION OF ABSTRACT:	18. NUMBER OF PAGES	19a. NAME OF RESPONSIBLE PERSON (Monitor)
a. REPORT	b. ABSTRACT	c. THIS PAGE			Kacey Blunck
Unclassified	Unclassified	Unclassified	SAR	38	19b. TELEPHONE NUMBER *(Include Area Code)* (937) 255-1305

Standard Form 298 (Rev. 8-98)
Prescribed by ANSI Std. Z39-18

EFFECT OF STRAIN-PATH REVERSAL ON MICROSTRUCTURE EVOLUTION AND CAVITATION DURING HOT TORSION TESTING OF Ti-6Al-4V

P. D. Nicolaou* and S.L. Semiatin

Air Force Research Laboratory, Materials and Manufacturing Directorate,
AFRL/MLLM, Wright-Patterson Air Force Base, OH 45433-7817, USA
*El. Venizelou 31, 191 00, Megara, GREECE
Tel. +30-229-602 5492, Fax, +30-229-602 5492, e-mail: NicolaouP@aget.gr

Abstract

Hot torsion testing comprising multiple twist reversals was used to establish the effect of strain-path changes on concurrent dynamic globularization and cavitation of Ti-6Al-4V with a colony-alpha starting microstructure. Optical microscopy was used to quantify the cavity area fraction and the effect of globularization on cavitation. The deformation of the hard and soft colonies surrounding the *largest* cavities and self-consistent-model calculations of strain partitioning were used to estimate the macroscopic and local strains at which colonies with different strengths globularize. It was found that both hard and soft colonies undergo dynamic globularization at the same *local* strain (i.e., strain within the colony). In addition, cavitation behavior during torsion with multiple strain-path changes was interpreted by taking into account the break up of the colonies into a globular structure. It was found that cavity growth (or shrinkage) persisted as long as there was a flow-stress difference in adjacent regions/colonies surrounding a given cavity. When the microstructure became uniform (as in the case of full globularization), the cavity area fraction did not change measurably with subsequent additional deformation.

I. INTRODUCTION

Two-phase, alpha/beta titanium alloys, such as Ti-6Al-4V, are usually processed via an ingot metallurgy route comprising working and heat treatment in the single-phase beta field followed by breakdown in the alpha/beta field of the colony microstructure thus produced. Open-die forging via cogging and upsetting is typically used for microstructure breakdown to obtain the desired equiaxed- alpha billet structure. From a macroscopic perspective, these industrial processes appear to be quite simple. At the microscale, however, they are very complicated, for they involve complex stress states, temperature variations, local microstructure changes (e.g., spheroidization, or globularization as it is known in the titanium industry), etc. In addition, there are often numerous changes in the strain-path, increasing the degree of complexity significantly. Depending on the specific ingot melting technique, final product size, working conditions, etc., wrought products may contain undesirable defects such as microstructure non-uniformities, shear bands, and internal cavities. The determination of the mechanisms that lead to the formation of such defects is very important for the design of economical thermomechanical processes, let alone for the manufacture of finished products with optimal service properties [1-4].

A considerable amount of research has been devoted to develop an understanding of cavitation behavior for a wide range of metals and alloys. Early work dealt primarily with conditions under which cavitation can be fully suppressed/minimized or establishing cavity-growth kinetics [5-8]. Later research focused on the effect of macroscopic stress state on cavitation kinetics. Usually, the stress state employed in these efforts resulted in a stress ratio (i.e., ratio of mean to effective stress) equal to or greater than that corresponding to uniaxial tension (i.e., 1/3). By contrast, Bae, et al. [9], and Nicolaou, et al. [10, 11] investigated cavitation

under macroscopic simple shear conditions. Most recently, Bieler, et al. [12] and Nicolaou and Semiatin [13] examined the effect of local texture and local stress state on non-uniform deformation and cavitation in alpha/beta titanium alloys with a colony-alpha microstructure. These efforts dealt with tension [12], compression [13], and torsional [10, 11] modes of deformation. The enhancement of cavitation due to the development of high triaxial stress in regions with colonies of different Taylor factors (and hence different strengths) was also quantified.

The objective of the current research was to develop a first-order understanding of the interaction of microstructure evolution and cavitation during the hot-working of titanium alloys with a colony-alpha microstructure deformed under complex strain-path conditions. For this purpose, hot torsion testing of Ti-6Al-4V with multiple reversals in twisting sense was used. The first part of the work delineated microstructure changes (i.e., dynamic globularization) within hard and soft colonies by exploiting the earlier finding that large cavities (which can be used as internal markers) develop between soft and hard colonies [12, 14]. The second part of the work consisted of an extension of previous hot torsion work in which deformation was either monotonic or comprised a single reversal [10, 11]. In the present effort, three and four-step torsion tests on the same Ti-6Al-4V alloy were conducted, and the effect of multiple strain-path changes on cavitation behavior was established.

II. MATERIALS AND PROCEDURES

Reversed hot torsion testing was used to establish the effect of strain-path changes on the interaction of microstructure changes and cavitation for a typical alpha/beta titanium alloy, Ti-6Al-4V. The material used in the present work was the same as in previous efforts [10, 11]. In brief, as-received, hot-rolled bar stock was beta annealed to produce relatively fine beta grains with a mixed colony, basketweave

microstructure. The beta grain size (and comparable colony size) was ~100 μm; the heat treatment also produced a grain-boundary alpha layer approximately 3 μm thick.

All of the hot torsion tests were conducted at 815°C using a twist rate that produced an effective strain rate equal to 0.04 s^{-1} at the outer surface of round-bar torsion specimens of the same geometry as in previous work. The different strain paths applied to the torsion specimens are described in Figure 1. For a given experiment, the strain increment for the forward (F) and reverse (R) deformation segments was the same. The surface effective strain increments were typically 0.99 (twist = 125°) or 1.78 (twist = 225°). Two, three, or four strain increments were imposed. There were two variations of the three-step tests; i.e., in the third step of some experiments, the twisting direction was changed from backward to forward, while in others the backward motion was continued throughout the third step. In all cases, the twisting direction was reversed quickly; the "dwell" time for the change of twisting direction was ~1-2 seconds between the steps.

After testing, *axial* (z) - *tangential* (θ) cross sections near the outer surface of the specimen (i.e., sections containing the z-θ plane) were prepared for metallographic examination. Microstructure evolution and cavitation were quantified as in the previous efforts [10, 11] using a combination of optical and scanning-electron microscopy and quantitative metallography.

III. RESULTS AND DISCUSSION

The key results from this work consisted of the determination and interpretation of plastic-flow response, globularization behavior, and cavitation during hot torsion.

A. *Plastic Flow Behavior*

Effective stress-effective strain curves for various three-step and four-step torsion tests are presented in Figures 2a (strain per step = 0.99) and 2b (strain per step = 1.78). The results for the first two steps are identical to those described previously for forward-reverse (two-step) torsion tests [11]. As before, the initial forward plastic flow behavior was characterized by a peak stress at very low strains (< 0.1) followed by marked flow *softening* (quantified by a negative strain-hardening exponent, n = –0.2). On the other hand, each reloading revealed a large reduction in the initial flow stress (relative to that at the end of the previous strain increment) followed by a relatively high rate of work *hardening* for a strain interval of ~0.2. After achieving a peak stress during the second and subsequent strain increments, a relatively small amount of flow softening in comparison to that observed during the initial forward step was noted.

The plastic-flow observations have been ascribed by Poths, et al. [15, 16] to a Bauschinger-like effect which has also been noted in a number of other materials such as stainless steel during hot working [17]. The specific explanation for the reloading transients in reversed torsion testing of the two-phase Ti-6Al-4V alloy, however, may lie in somewhat different microscopic slip processes compared to single-phase alloys with equiaxed grain structures. Specifically, the initial flow softening (at low strains) has been ascribed to slip transfer across the alpha-beta interfaces. When the deformation is reversed, there may be a large number of mobile dislocations which can move easily in the reverse direction. Because the original alpha-beta interfaces have now been broached, it may be easier to form subgrain-like substructures in both the alpha and beta phases, thus leading to an initial strain-hardening transient

followed by near steady-state flow as in single-phase metals whose flow is controlled dynamic recovery.

B. *Microstructure Evolution*

1. *Globularization observations*

As is discussed in Section III.B.2, globularization observations focused on regions with cavities because of the ability to estimate local strains in such areas. Typical optical micrographs, which indicate globularization on one side or all around a large cavity, are shown in Figure 3. Figure 3a (corresponding to a monotonic torsion test with a twist angle of 125°) shows a globular microstructure along one side of the cavity, which is assumed to be a soft (more highly deformable) colony. Figure 3b (corresponding to another monotonic test with a twist angle of 250°) shows a globular structure which entirely surrounds a large cavity. Similar observations were made for other testing conditions (i.e., different strain paths).

The results of the metallographic examination for the various testing conditions are summarized in Table I. Specifically, for the monotonic tests, globularization of the soft colonies occurred at a macroscopic strain of 0.99 (125° twist); for the hard colonies, this strain increased to 1.98 (250° twist). When the straining direction was reversed, the macroscopic effective strain for globularization of the soft and hard colonies was 1.43 and 3.56, respectively.

2. *Determination of globularization strains*

The interpretation of microstructure evolution via dynamic globularization of the colony microstructure required the determination of local strains. This was accomplished by (i) identifying regions with hard *and* soft colonies that had undergone globularization and (ii) estimating the strain non-uniformity in such regions. Regions of interest were determined based on previous observations [10, 12]

that the largest cavities were present in areas having adjacent hard *and* soft colonies. In other words, large cavities were usually surrounded by one (or more) hard colonies on one side and soft colonies on the other. Hence, dynamic globularization strains were estimated by focusing on the regions containing large cavities.

The local strains accommodated by hard and the soft colonies as a function of the externally imposed (macroscopic) strain were estimated using a self-consistent-model [18]. As in previous work, the strength differences between colonies was assumed to arise from differences in the Taylor factor of the alpha lamellae, which comprise ~80 pct. of the two-phase microstructure at 815°C. Model calculations assuming a strain-rate sensitivity of 0.15, volume fractions of the hard and soft colonies equal to 60 and 40 pct., respectively, and two different ratios of the Taylor factors of the hard and soft colonies (i.e., $M_h/M_s = 2$ or 3) are shown in Figure 4. No "intermediate" strength colonies were considered in the calculations. The application of the self-consistent model in cavitated regions is approximate because of the generation of traction-free surfaces during cavity growth. Hence, the strain non-uniformity so estimated would tend to be liberal.

The local (colony) strain at which the soft and the hard colonies were globularized, estimated by coupling the self-consistent model calculations (Figure 4) and the experimental observations (Table I), are summarized in Figure 5 for both monotonic and reversed types of torsion tests. The individual data points correspond to the average of the self-consistent-model strain estimates for Taylor factor ratios (M_h/M_s) of 2 and 3; the error bars indicate the spread between the results for these two values of the Taylor-factor ratio. For a given straining mode (i.e., monotonic or reversed), Figure 5 suggests that the local colony strain for globularization is somewhat higher for soft colonies compared to that for hard colonies. However, the

difference is not great and may be rationalized on the basis of the model assumptions. Thus, the *local* strains at which colonies globularized may be concluded to be essentially the same irrespective of Taylor factor.

The finding concerning the similarity in local strains for dynamic globularization is somewhat unexpected in view of the definition of the Taylor factor, $M = \Sigma\gamma_i/\varepsilon$, in which ε represents the imposed strain (in the present case, the so-called *local* strain), and $\Sigma\gamma_i$ denotes the total *internal (crystallographic) shear strain*. Such a strain-based definition of M, often used for cubic materials, is not as simple for hcp materials (due to various different types of slip systems). Nevertheless, it appears at least qualitatively that hard colonies (with their larger values of M) require more crystallographic shear than soft colonies (with smaller M) in view of the nearly identical levels of ε for both hard and soft colonies. Although crystallographic shear certainly plays an important role in the dynamic-globularization process [19], the *uniformity* of shear along the length of the alpha platelets (implicitly assumed in Taylor-type models) must also be considered. Based on the observations of Bieler and Semiatin [20], it may be hypothesized that the degree of strain localization may be smaller for soft colonies (in which prism <a> and basal <a> systems are activated) compared to that in hard colonies (in which pyramidal <c+a> slip is activated). For this reason, the *uniform* break-up of soft colonies may be more readily accomplished than for hard colonies. However, further detailed research is needed to verify this hypothesis.

The present results were also interpreted in the context of previous research conducted by Poths, et al. [15, 16]. In this previous work, the dynamic globularization kinetics for Ti-6Al-4V with a colony-alpha microstructure were determined as a function of strain path in torsion. It was found that the globularized

fraction shows a measurable dependence on the strain path (Figure 6). Specifically, at a given total effective strain $\bar{\varepsilon}$, the globularized fraction was *higher* for a monotonic loading mode relative to that for the case in which the straining (twisting sense) was reversed at a strain of $\bar{\varepsilon}/2$. On the other hand, the globularization behavior was essentially identical for deformations involving one or two reversals in twisting direction (i.e., two-step or three-step tests, respectively). These results were interpreted using the following arguments: (i) Strain-path reversal results in a reduced rate of dislocation multiplication relative to that for a monotonic deformation because of the reduced interaction of dislocations with obstacles such as alpha/beta interfaces. The rate of recovery and thus formation of sub-boundaries is thereby reduced. (ii) The misorientations across sub-boundaries formed during deformation involving a strain-path reversal would also be less, thus reducing the boundary energy and, hence, the boundary-splitting (grooving) rate. (iii) The formation of shear bands and shear "offsets" due to slip transfer across the α-β boundaries is also retarded by the strain reversal [16].

The present measurements of the *macroscopic* strains for dynamic globularization of hard and soft colonies (shaded ovals in Figure 6) were compared to the measurements of Poths, et al. [15]. For each pair of shaded ovals, the left one refers to monotonic torsion and the right one to reversed torsion. For *monotonic* loading, the soft colonies globularized at small macroscopic strains inasmuch as they accumulated a relatively large amount of strain on a local scale for a given increment of macroscopic strain, while the hard colonies globularized near a macroscopic strain at which almost the entire microstructure is globularized. The corresponding points showed excellent agreement with the monotonic curve of Poths, et al. For the *reversed* loading conditions, the corresponding soft and hard colony strains showed

very good direct agreement with the *measured* reversed-torsion curve of Poths, et al. (soft colonies) as well as an *extrapolation* of the curve to large strains (for the hard colonies). These results demonstrate that effective strains of the order of 3.5 are required to achieve full dynamic globularization of the microstructure when the strain direction is reversed.

C. *Cavitation*

1. *Cavity-fraction measurements*

The variation of the cavity area fraction C_A and the average cavity size (radius) as a function of the imposed macroscopic strain and strain path in four-step experiments is shown in Figure 7. The relatively sharp drop in cavity fraction and size which happens during the first strain-path reversal has been analyzed in detail in Reference 11. Of interest here is the behavior during the next two steps, i.e., the cavitation during further subsequent forward and then reverse strain increments. Two different behaviors, depending on the magnitude of the imposed strain increments, were observed. For the lower strain-increment tests (effective surface strain of 0.99, or 125° twist), there was an *increase* in cavity fraction and size during the second forward step (third step overall) and a decrease during the second reversal (fourth step overall). On the other hand, for the higher strain-increment tests (effective strain of 1.78, or 225° twist), the cavity fraction and size remained essentially unchanged during both the third and fourth steps.

The dependence of cavity area fraction on strain path is further elucidated in Figure 8 for hot torsion tests comprising three increments of strain, each of which equaled 0.99. In one case, the strain path was changed from reverse to forward for the third strain increment, and in the other experiment it was not. The results revealed that C_A *increased* during the third step when the straining direction was changed from

reverse to forward, albeit at a slower pace compared to the first forward step. By contrast, C_A changed very little when the strain direction remained in the reverse mode. These observations have been discussed in Reference 11, and the small change is attributed to the retardation of the densification rate with strain at the latter stages of pore closure. Specifically, both experimental findings as well as densification models for powder consolidation [21-23] show that the densification rate decreases mainly due to the decrease of the stress intensification factor as well as the increase in Poisson's ratio with an increase of the relative density.

2. *Qualitative effect of stress triaxiality on cavity growth/shrinkage*

The observations described in Figures 7 and 8 were interpreted *qualitatively* in terms of the change in stress triaxiality that accompanied the breakdown of the colony-alpha microstructure.

As discussed previously [8, 9], the cavity-growth rate is greatly influenced by stress triaxiality, i.e., the ratio of the mean to effective stress. The local stress triaxiality (i.e., at the colony scale) is the result of two contributing factors: (i) the externally applied stress state and (ii) the orientation of adjacent colonies with respect to the principal axes of the external stress state. In the case of simple shear, the contribution of the external stresses is null. Therefore, any finite stress triaxiality responsible for cavity growth is due solely to local texture effects.

When adjacent cavities are oriented such that their Taylor factors differ greatly, the stress triaxiality is high. If the two colonies are of the same orientation, the stress triaxiality is zero. Thus, rapid cavity growth is favored in the former case, while no such growth would take place in the latter.

During the hot torsion tests for Ti-6Al-4V with a colony-alpha starting microstructure, the stress triaxiality did not remain constant throughout the

deformation and cavitation processes. There were two factors that tended to *decrease* the stress triaxiality, (i) cavity growth and (ii) changes in the microstructure. As a cavity grew, the degree of plastic constraint imposed by colonies with different flow properties decreased. Thus, the tensile and compressive stresses generated in the softer and harder colonies, respectively, decreased gradually, and therefore the cavity-growth rate decreased as well. Furthermore, when the colonies globularized, the degree of microstructural/textural non-uniformity around a cavity decreased. As a result, the flow stress difference between the two colonies decreased, the stress triaxiality was reduced to zero, and hence cavity growth (or shrinkage) tended to cease.

Figure 9 shows the microstructures developed around cavities during forward-reverse-forward torsion for strain increments of 0.99 or 1.78. In Figure 9a (strain increments of 0.99), the colony structure was preserved on one side of the cavity, while in Figure 9b, the microstructure around the cavity was fully globular. As a result, one might expect a change in the cavity area fraction (and cavity size) with strain for the smaller strain increment, as was indeed found (Figure 7a), while the amount of cavitation would be expected to remain constant for the larger strain increment, as was also confirmed experimentally (Figure 7b).

3. *Quantitative analysis of cavity growth/shrinkage*

The results shown in Figures 7 and 8 were also interpreted *quantitatively* using the model described previously [10, 11]. In particular, the AFRL powder-densification model [20] was employed for the "reverse" steps, i.e., the (F)-R and (F-R-F)-R stages, in which cavities tended to shrink. For the third, forward-deformation, step (i.e. (F-R)-F), this model cannot be just simply reversed to account for the *growth*

of internal cavities. In this instance, therefore, the following, more traditional, cavity-growth equation was used:

$$C_A = C_{Ao} \exp\left(\eta_A \left(\bar{\varepsilon} - \bar{\varepsilon}_o\right)\right) \quad (1)$$

Here, C_A denotes the cavity area fraction at an effective strain $\bar{\varepsilon}$, C_{Ao} is the fraction at a strain $\bar{\varepsilon}_o$, and η_A is the areal cavity-growth rate.

The experimental results for the cavity area fraction at the end of each step in the torsion tests have been redrawn in Figure 10. The first part of each of the two graphs (i.e. the (F)-R steps) was analyzed in Reference 11. In this previous work, it was concluded that predictions assuming a "stationary" or a fully-rotating microstructure bounded the measurements. The two-step torsion-test results were bounded well using a Taylor-factor ratio of M_h/M_s=3 for the strain increment of 0.99, while they were bounded using M_h/M_s=2 for the larger strain increment (1.78). This trend may be attributed to the different microstructural changes (globularization) associated with the two strain increments as discussed in Section III.B.

Focusing in more detail on the results for the strain increment of 0.99 (Figure 10a), cavity *growth* during the (F-R)-F step was modeled using Equation (1). In Reference 10, the cavity-growth rate during the first step of forward deformation, during which substantial flow softening occurred, was found to be equal to 0.75. In contrast, for the (F-R)-F step in which flow hardening/softening is essentially zero, the stress triaxiality factor $\sigma_m/\bar{\sigma}$ is lower (0.12 vs. 0.17). Thus, the ratio of η's for the (F-R)-F and "F" steps is found to be equal to ~0.8. The cavity-growth behavior for the (F-R)-F step in Figure 10a thus corresponds to Equation (1) with η = 0.6 (= 0.75 x 0.8). For the final ((F-R-F)-R) step in Figure 10a in which cavity *shrinkage* occurs, the decrease of stress triaxiality associated with globularization was evidenced by the fact that the experimental results were bounded by the rotation/no-rotation

curves for M_h/M_s =2. The corresponding curves for M_h/M_s = 3 (not shown for clarity) broadly underestimated the final level of cavitation.

For the strain increment of 1.78 (Figure 10b), the microstructure surrounding the cavities after the (F-R) step was relatively uniform due to globularization. Therefore, the stress triaxiality was zero, and cavitation would be predicted to remain unchanged, as was observed.

IV. SUMMARY

Multi-step hot torsion tests, in which the strain was reversed after each step, were conducted in order to investigate concurrent dynamic globularization and cavitation behavior of Ti-6Al-4V with a colony-alpha starting microstructure. The observation that the largest cavities develop in regions with both soft and hard colonies was exploited to determine the local (colony-scale) strains at which colonies with different strengths (due to their different Taylor factors) globularize. Using self-consistent model calculations of local strains, it was found that both hard and soft colonies require the same local strain, at least to a first order, in order to globularize. Cavitation behavior was interpreted by taking into account the break up of the colonies into a globular structure. It was found that growth or shrinkage of a cavity occurred as long as there was a flow stress difference in the adjacent regions that surrounded it. When the microstructure became uniform, as in the case of full globularization, the cavity fraction remained constant and did not change noticeably with further deformation.

Acknowledgements- This work was conducted as part of the in-house research activities of the Metals Processing Group of the Air Force Research Laboratory's Material and Manufacturing Directorate. The support and encouragement of the laboratory management and the Air Force Office of Scientific Research (Capt. Brett Conner, program manager) are gratefully acknowledged. One of the authors (PDN) was supported under Air Force contract FA8650-04-D-5235. The assistance of Messrs. P.N. Fagin and J.D. Miller in conducting the torsion tests is highly appreciated.

REFERENCES

1. S.L. Semiatin, V. Seetharaman, and I.Weiss: in *Advances in the Science and Technology of Titanium Alloy Processing*, I. Weiss, R.Srinivasan, P.J. Bania, D. Eylon, and S.L. Semiatin, eds., TMS, Warrendale, PA , 1997, pp. 3-73.

2. S.L. Semiatin, V. Seetharaman, and I. Weiss: *Mater. Sci. Eng. A*, 1999, vol. A263, pp. 257-71.

3. S.L. Semiatin, R.L. Goetz, E.B. Shell, V. Seetharaman, and A.K. Ghosh: *Metall. Mater. Trans. A*, 1999, vol. 30A, pp. 1411-1424.

4. J.C. Williams and E.A. Starke, Jr.: in *Deformation, Processing, and Structure*, ASM, Metals Park, OH, 1982, Chapter 7.

5. M.J. Stowell: in *Superplastic Forming of Structural Alloys*, N.E. Paton and C.H. Hamilton, eds., TMS-AIME, Warrendale, PA, 1982, pp. 321-26.

6. C.C. Bampton and J.W. Edington: *J. Eng. Mater. Techn.*, 1983, vol. 105, pp. 55-60.

7. R. Verma, P.A. Friedman, A.K. Ghosh, S. Kim, and C. Kim: *Metall. Mater. Trans. A*, 1996, vol. 27A, pp. 1889-1898.

8. P.D. Nicolaou, S.L. Semiatin, and A.K. Ghosh: *Metall. Mater. Trans. A*, 2004, vol. 35A, pp. 2187-2190.

9. D.H. Bae, A.K. Ghosh, and J.R. Bradley: *Metall. Mater. Trans. A*, 2003, vol. 34A, pp. 2449-2463.

10. P.D. Nicolaou, J.D. Miller, and S.L. Semiatin: *Metall. Mater. Trans. A*, 2005, vol. 36A, pp. 3461-3469.

11. P.D. Nicolaou and S.L. Semiatin: *Metall. Mater. Trans. A*, 2006, vol. 37A, in press.

12. T.R. Bieler, P.D. Nicolaou, and S.L. Semiatin: *Metall. Mater. Trans. A*, 2005, vol. 36A, pp. 129-140.

13. P.D. Nicolaou and S.L. Semiatin: *Metall. Mater. Trans. A*, 2005, vol. 36A, pp. 1567-1574.

14. T.R. Bieler, R.L. Goetz, and S.L. Semiatin: *Mater. Sci. Eng. A.*, 2005, vol. A405, pp. 201–213.

15. R.M. Poths, G. Angella, B.P. Wynne, W.M. Rainforth, S.L. Semiatin, and J.H. Beynon: *Metall. Mater. Trans. A*, 2004, vol. 35A, pp. 2993-3001.

16. R.M. Poths, B.P. Wynne, W.M. Rainforth, S.L. Semiatin, and J.H. Beynon: in *Ti-2003: Science and Technology*, G. Luetjering and J. Albrecht, eds., Wiley-VCH Verlag GmbH, Weinheim, Germany, 2004, pp. 1243-1250.

17. G. Angella, B.P. Wynne, J.H. Beynon, and W.M. Rainforth: in *THERMEC'2000*, T. Chandra, K. Higashi, C. Suryanarayana, and C. Tome, eds., Elsevier Science, published on CD, 2000.

18. S.L. Semiatin, F. Montheillet, G. Shen, and J.J. Jonas: *Metall. Mater. Trans. A*, 2002, vol. 33A, pp. 2719-2727.

19. I. Weiss, G.E. Welsch, F.H. Froes, and D. Eylon: in *Titanium: Science and Technology*, G. Luetjering, U. Zwicker, and W. Bunk, eds., Deutsche Gesellschaft fr Metallkunde e.V., Oberursel, Germany , 1985, pp. 1503-1510.

20. T.R. Bieler and S.L. Semiatin: *International Journal of Plasticity*, 2002, vol. 18, pp. 1165-1189.

21. Y.-M. Liu, H.N.G. Wadley, and J.M. Duva: Acta Metall. Mater., 1994, vol. 42, pp. 2247-2260.

22. D.P. DeLo, R.E. Dutton, S.L. Semiatin, and H.R. Piehler: Acta Mater., 1999, vol. 47, pp. 3159-3167.

23. S. Shamasundar, R.E. Dutton, and S.L. Semiatin: Scripta Metall. Mater., 1994, vol. 31, pp. 521-525.

Table I. Gloularization Observations for Hot Torsion Tests on Ti-6Al-4V

		Globularization	
Twist Angle (Deg)	**Total Macroscopic Strain**	**Soft**	**Hard**
+125	0.99	Yes	No
+250	1.98	Yes	Yes
+225-225	3.56	Yes	Yes
+125-125+125	2.97	Yes	No
+225-225+225	5.34	Yes	Yes

Figure Captions

Figure 1. Schematic summary of the Ti-6Al-4V reversed hot torsion tests conducted in the present work. F refers to forward and B to backward twisting during torsion.

Figure 2. Effective stress-effective strain curves determined from torsion tests with multiple reversals of twisting direction. The surface effective strain for each increment of deformation was (a) 0.99 or (b) 1.78.

Figure 3. Microstructures developed around large cavities during monotonic torsion tests at 815°C and twist angles of (a) 125° or (b) 250°.

Figure 4. Self-consistent model calculations of the local effective strain developed in hard and soft colonies as a function of the macroscopic strain assuming a strain-rate sensitivity of 0.15 and a Taylor-factor ratio (M_h/M_s) of 2 or 3.

Figure 5. Local effective strains for dynamic globularization of the colony-alpha microstructure deformed via monotonic or reversed torsion testing at 815°C and a surface effective strain rate of 0.04 s^{-1}.

Figure 6. Comparison of the measured dynamic globularization kinetics from the work of Poths, et al. [15] (data points and trend lines) with those for soft and hard colonies determined in the present work (shaded ovals).

Figure 7. Variation of cavity area fraction and cavity size (radius) during hot torsion tests comprising two forward and two reverse stages. The effective strain increments for each deformation step were (a) 0.99 or (b) 1.78.

Figure 8. Cavity area-fraction measurements for three-step torsion tests (with a strain increment of 0.99) comprising a final (third) step that was imposed in either the forward direction or the reverse direction.

Figure 9. Microstructures developed around cavities in forward-reverse-forward hot torsion tests using a strain increment of (a) 0.99 or (b) 1.78.

Figure 10. Comparison of model predictions and experimental measurements of the cavity area fraction developed during hot torsion tests comprising two forward and two reverse stages. The effective strain increments for each deformation step were (a) 0.99 or (b) 1.78.

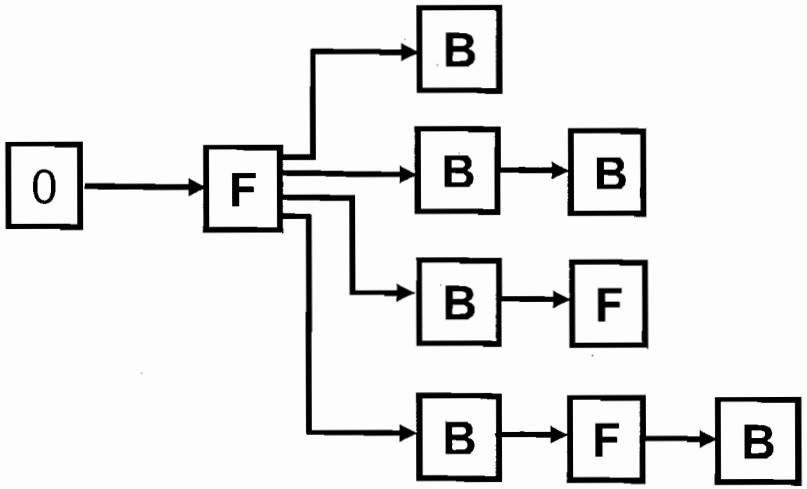

FIGURE 1

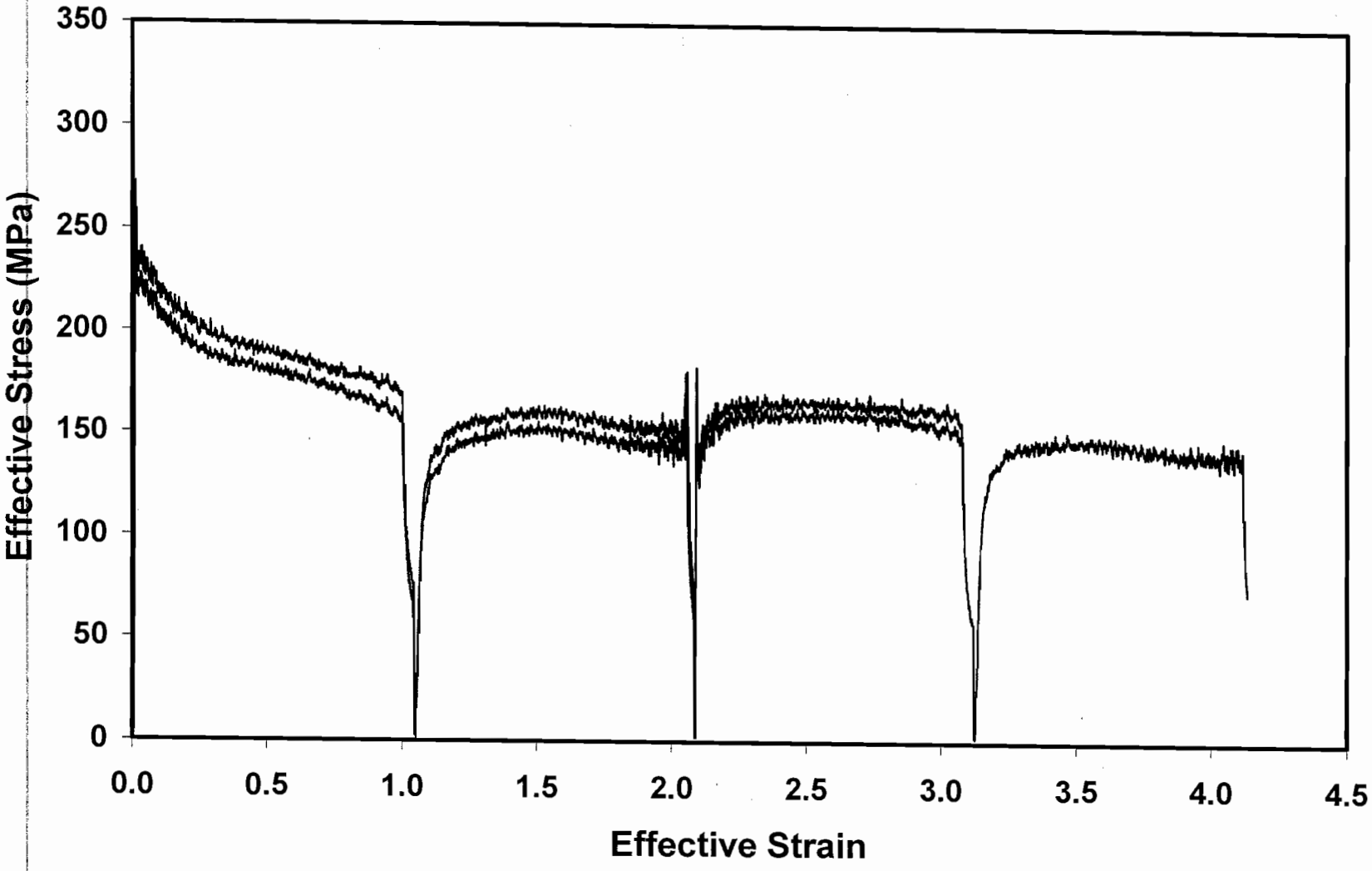
Effective Stress (MPa)
350
300
250
200
150
100
50
0
0.0
0.5
1.0
1.5
2.0
2.5
3.0
3.5
4.0
4.5
Effective Strain

FIGURE 2a

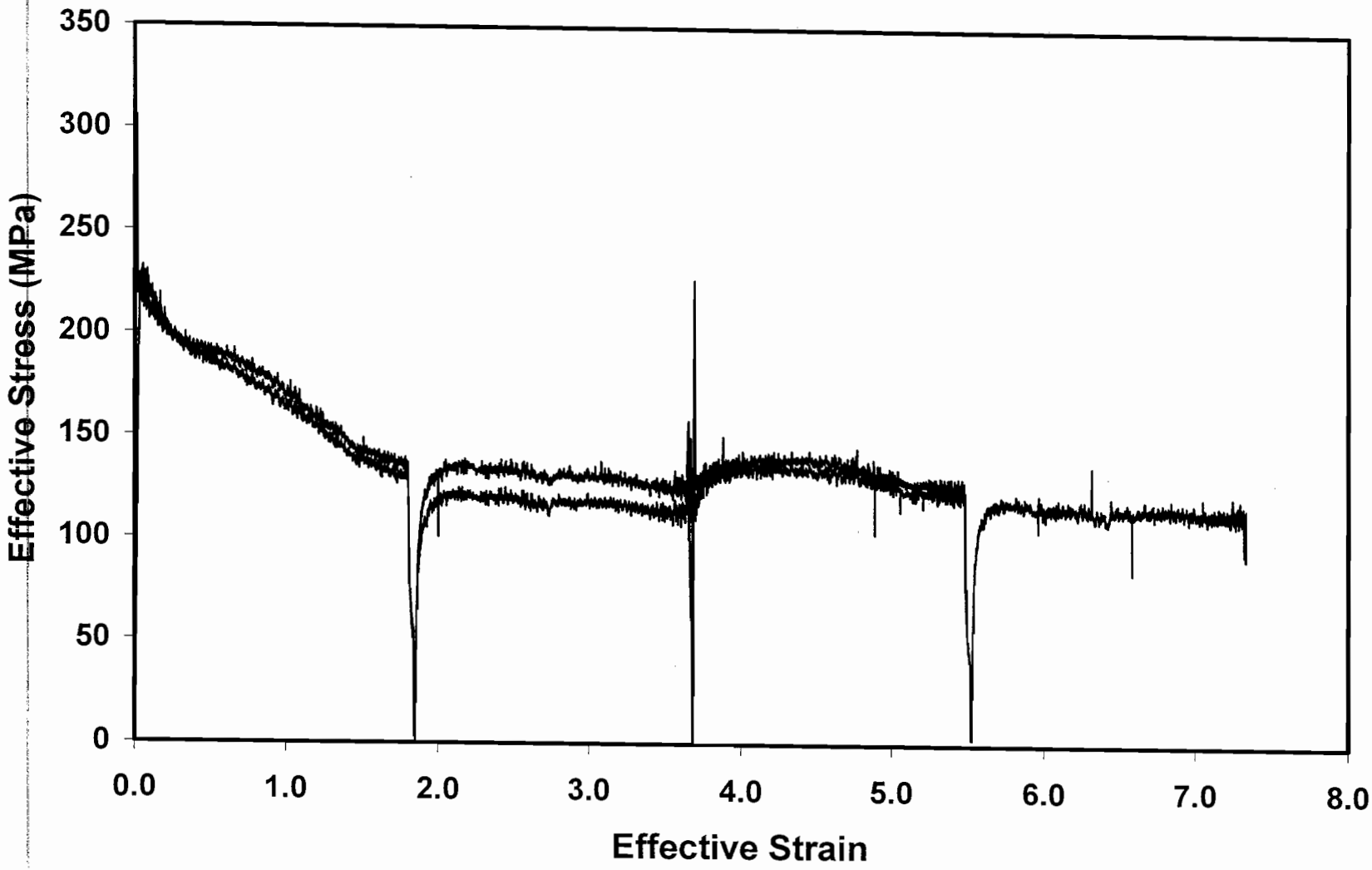
Effective Stress (MPa)
350
300
250
200
150
100
50
0
0.0
1.0
2.0
3.0
4.0
5.0
6.0
7.0
8.0
Effective Strain

FIGURE 2b

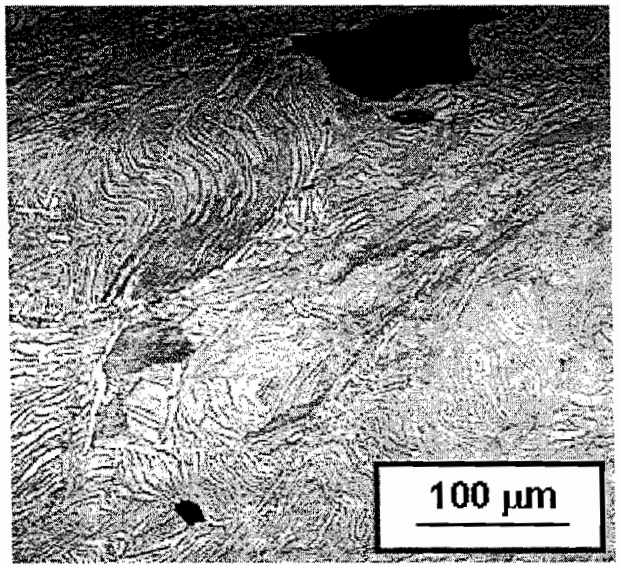

(a)

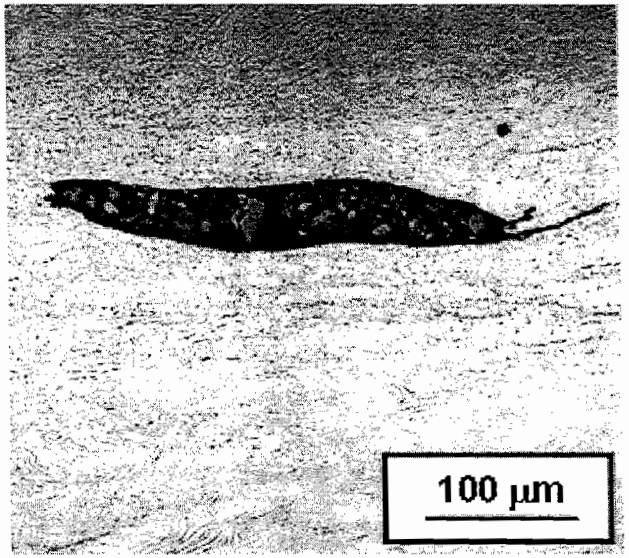

(b).

FIGURE 3

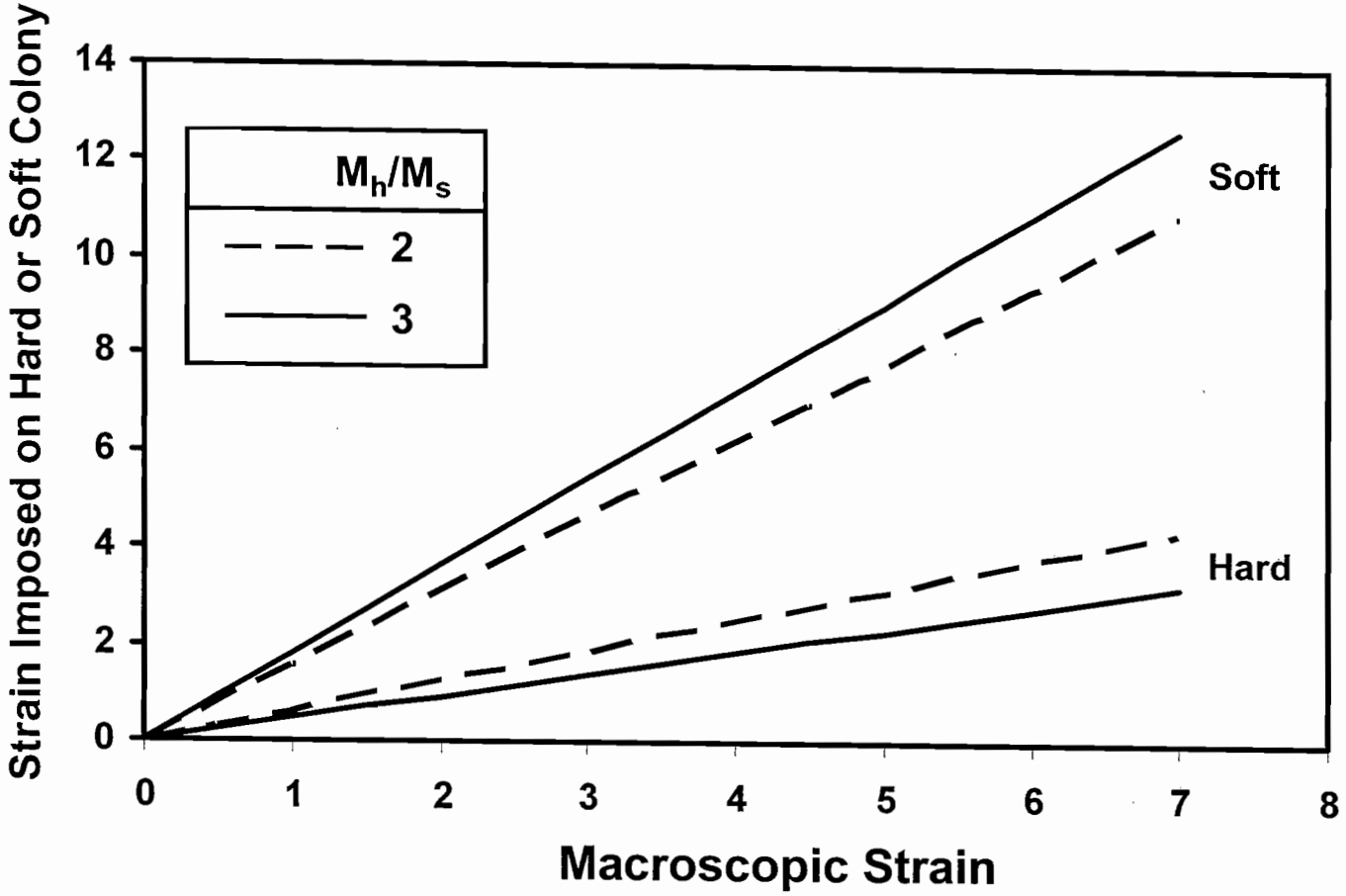
Strain Imposed on Hard or Soft Colony
14
12
10
8
6
4
2
0
0
1
2
3
4
5
6
7
8
Macroscopic Strain
M_h/M_s
2
3
Soft
Hard

FIGURE 4

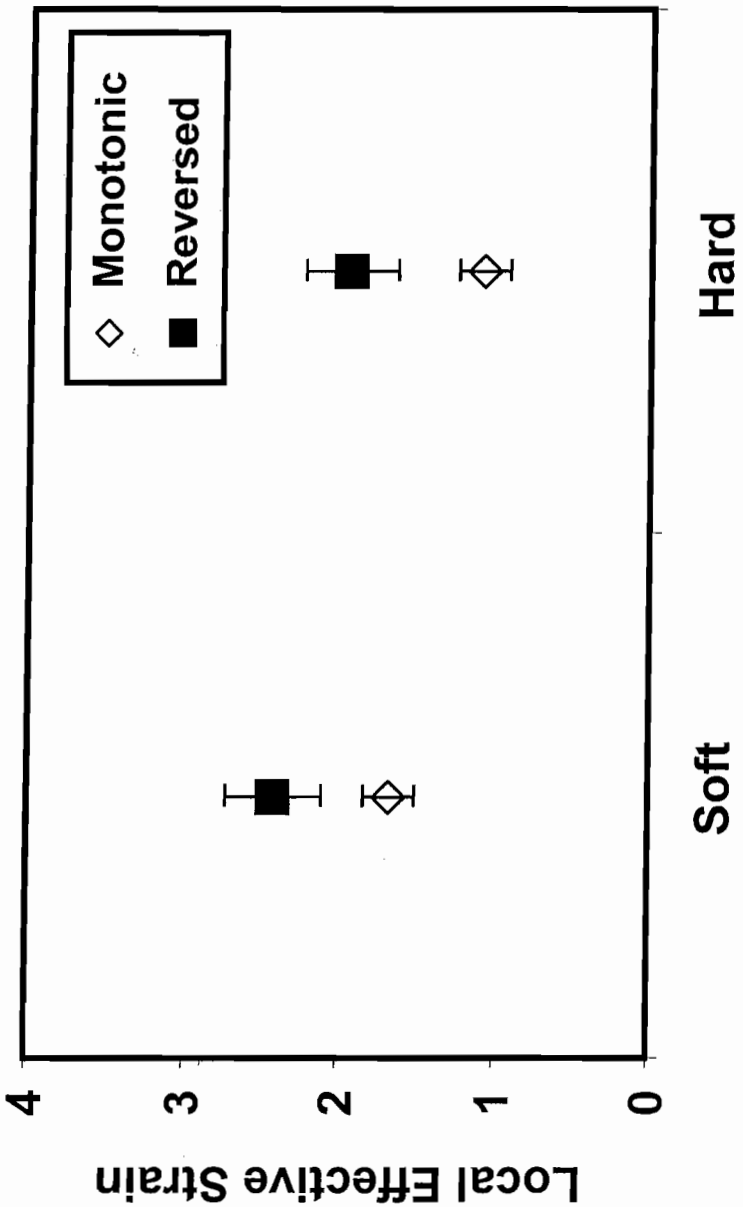
Local Effective Strain
0
1
2
3
4
Soft
Hard
Monotonic
Reversed

FIGURE 5

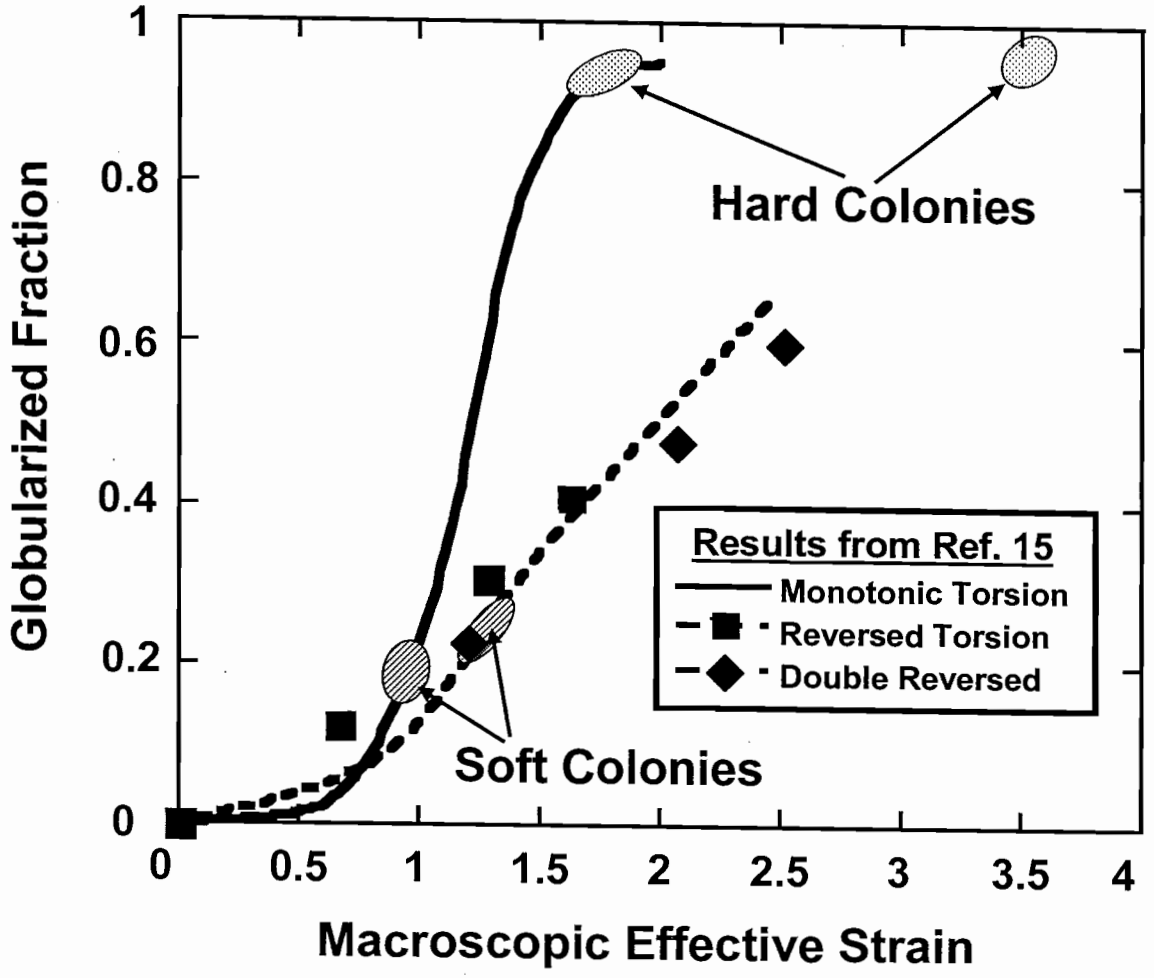
Globularized Fraction
Macroscopic Effective Strain
0
0.2
0.4
0.6
0.8
1
0
0.5
1
1.5
2
2.5
3
3.5
4
Hard Colonies
Soft Colonies
Results from Ref. 15
Monotonic Torsion
Reversed Torsion
Double Reversed

FIGURE 6

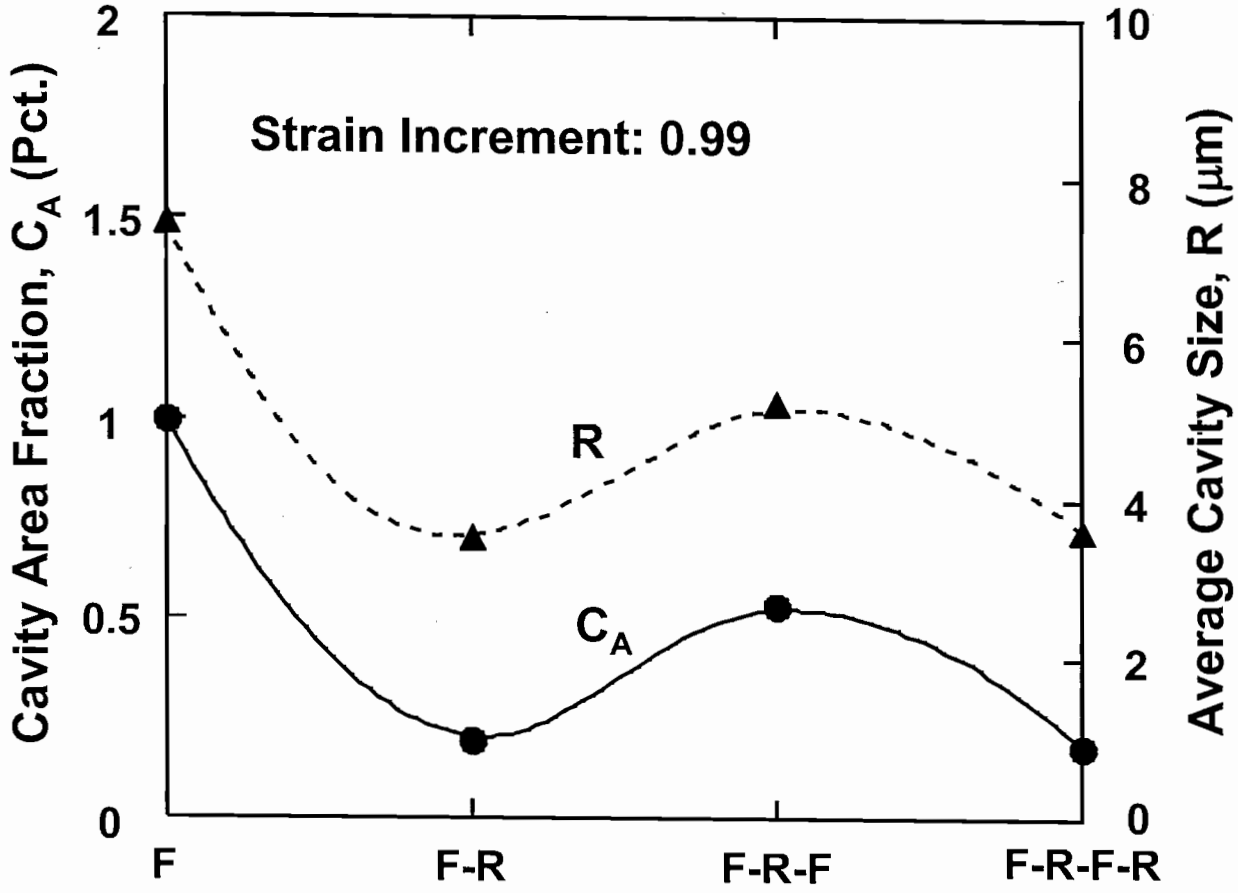
Strain Increment: 0.99
Cavity Area Fraction, C_A (Pct.)
Average Cavity Size, R (μm)
R
C_A
2
1.5
1
0.5
0
10
8
6
4
2
0
F
F-R
F-R-F
F-R-F-R

FIGURE 7a

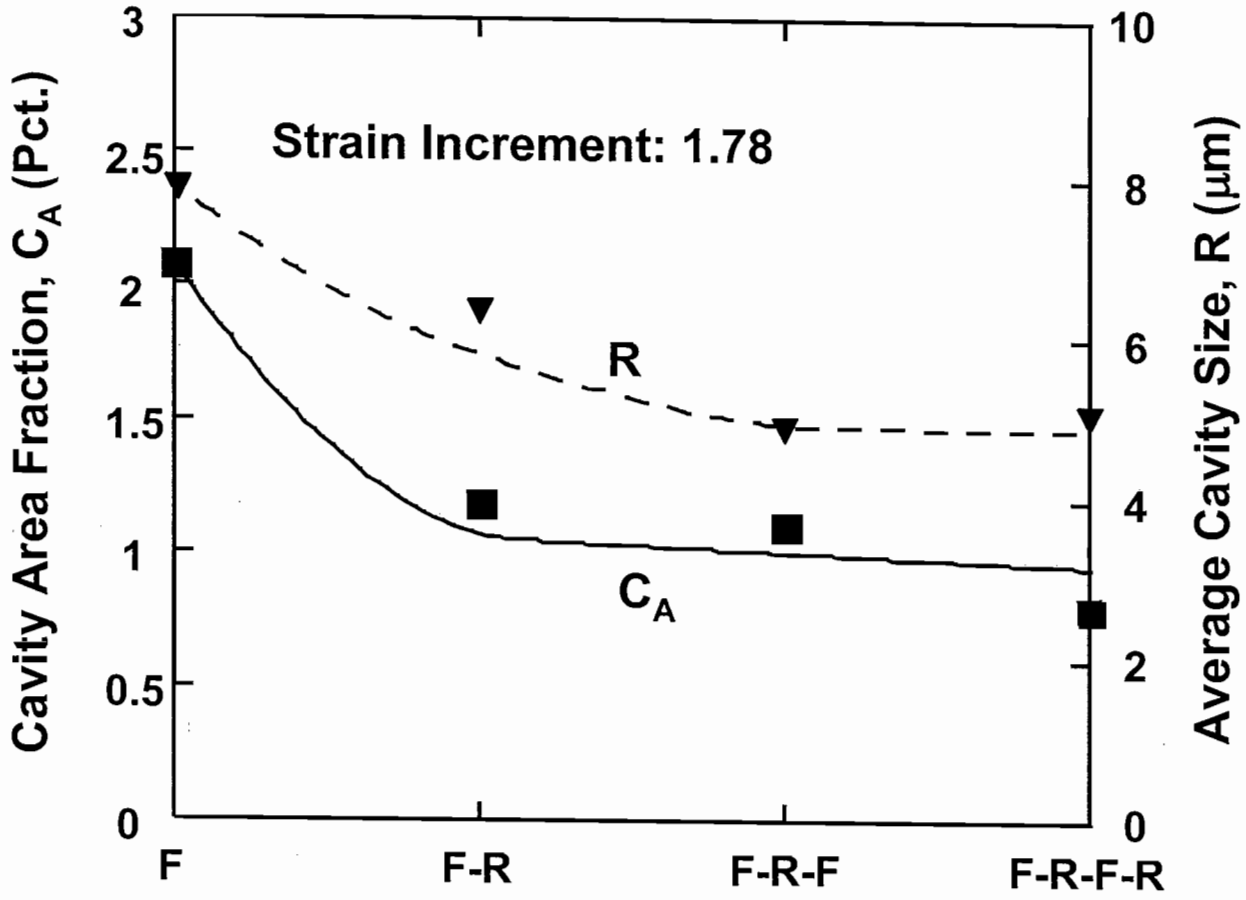
Strain Increment: 1.78
R
C_A
Cavity Area Fraction, C_A (Pct.)
Average Cavity Size, R (μm)
3
2.5
2
1.5
1
0.5
0
10
8
6
4
2
0
F
F-R
F-R-F
F-R-F-R

FIGURE 7b

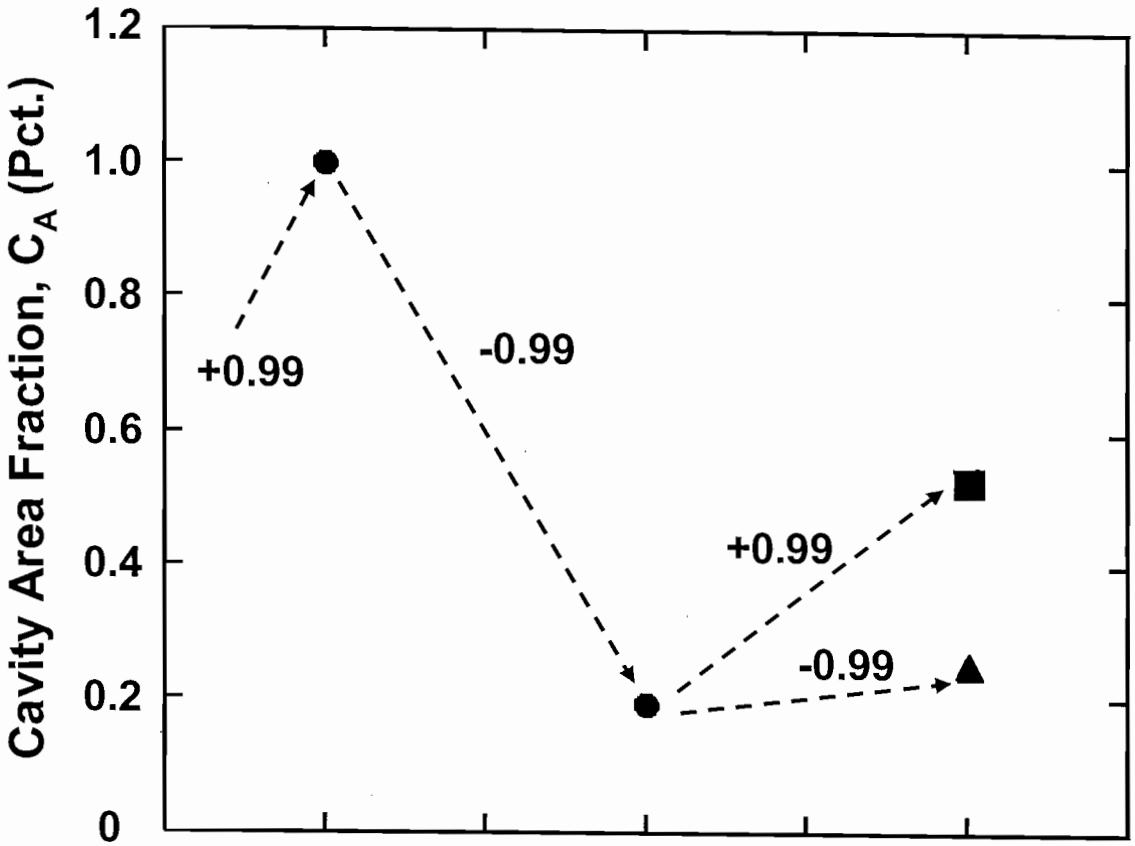

FIGURE 8

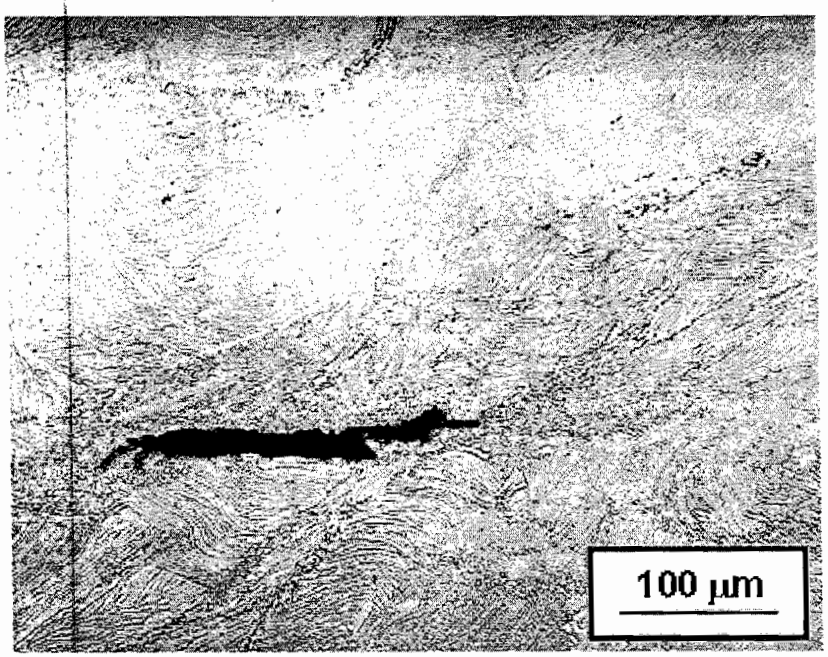

(a)

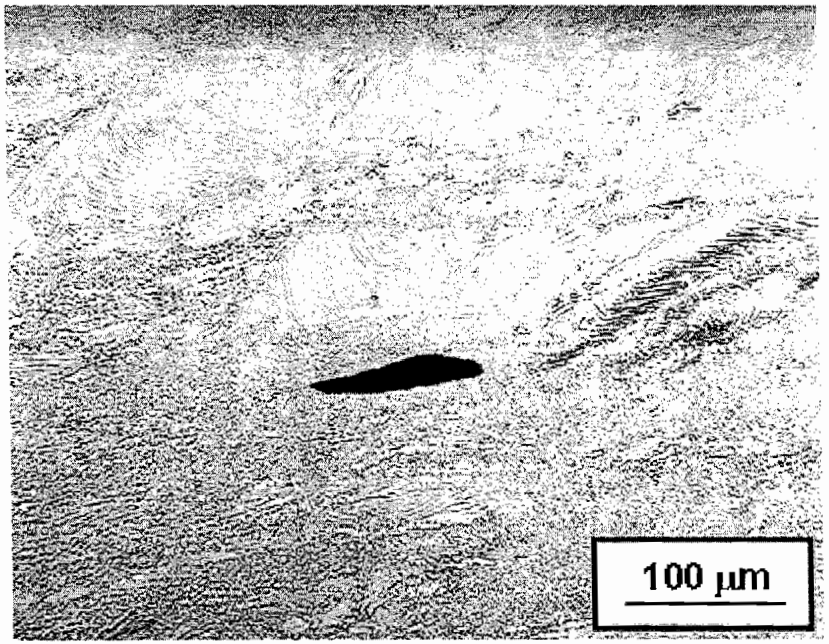

(b)

FIGURE 9

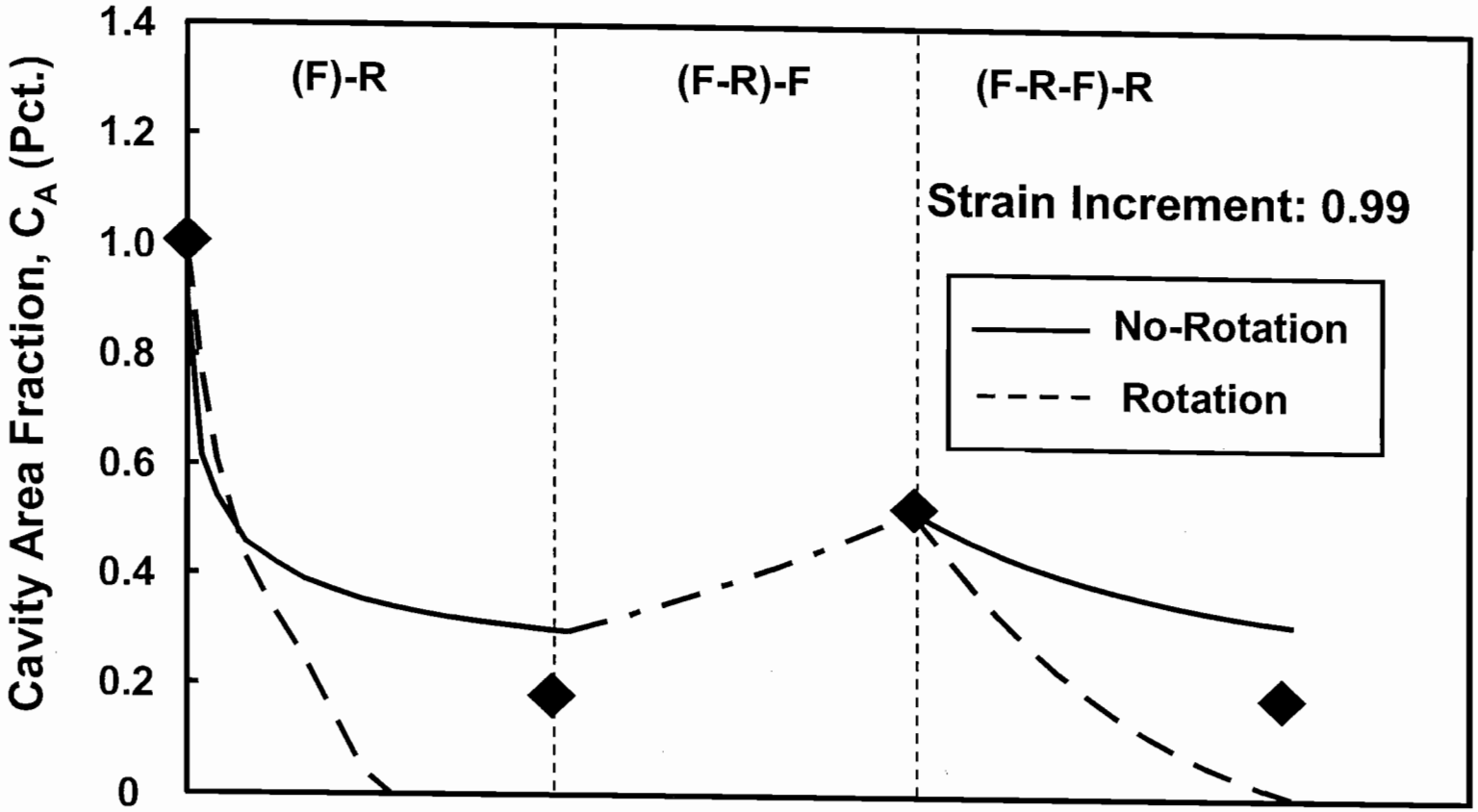
Cavity Area Fraction, C_A (Pct.)
1.4
1.2
1.0
0.8
0.6
0.4
0.2
0
(F)-R
(F-R)-F
(F-R-F)-R
Strain Increment: 0.99
No-Rotation
Rotation

FIGURE 10a

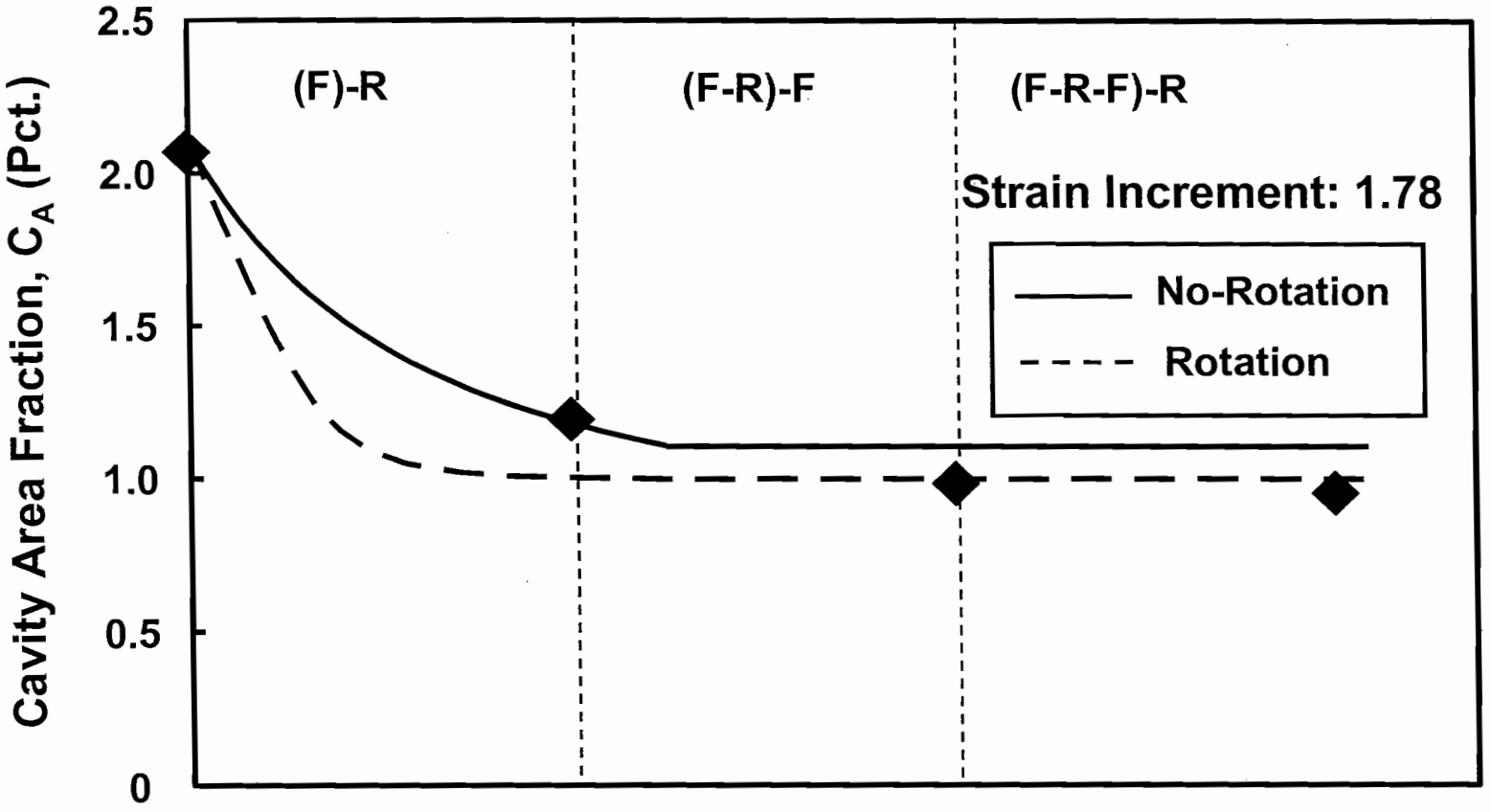
2.5
2.0
1.5
1.0
0.5
0
Cavity Area Fraction, C_A (Pct.)
(F)-R
(F-R)-F
(F-R-F)-R
Strain Increment: 1.78
No-Rotation
Rotation

FIGURE 10b